In situ ATR-FTIR study of oxygen reduction at the Pt/Nafion interface

K. Kunimatsu,[a] T. Yoda,[b] D. A. Tryk,[a] H. Uchida[ac] and M. Watanabe*[a]

Received 22nd August 2009, Accepted 1st October 2009
First published as an Advance Article on the web 12th November 2009
DOI: 10.1039/b917306d

We have developed a new half-membrane-electrode assembly (MEA)-type cell that allows us to conduct attenuated total reflectance–Fourier transform infrared (ATR-FTIR) measurements at the Pt/Nafion interface under humidified N_2/O_2 atmosphere. The cell consists of a gas-diffusion type anode placed on a carbon separator with a gas flow field, a Pt film cathode deposited chemically on an Si ATR prism and a Nafion NRE®211 electrolyte sandwiched between them. The construction allows the control of the atmosphere at the cathode by those at the anode *via* the electrolyte of 20-μm thickness.

An infrared absorption band was observed at 1400–1403 cm^{-1} under humidified oxygen atmosphere in close association with the appearance of ORR current. Its absence under N_2 atmosphere and insensitivity to the change from H_2O to D_2O humidification led us to ascribe the band to the O–O vibration of the adsorbed oxygen molecule O_2(ads). The band intensity increased with increasing ORR current but decreased significantly in the limiting current region. However, the stability of the species at potentials as high as 1.1 V *vs.* the reversible hydrogen electrode (RHE) led us to rule out the possibility that the band could be due to adsorbed superoxide O_2^-.

1. Introduction

The polymer electrolyte fuel cell (PEFC) has attracted global interest as a potential candidate for clean power sources for automobile, residential and portable applications. The cathodic overpotential for the oxygen reduction reaction (ORR) decreases the cell efficiency up to *ca.* 50% under practical current load conditions on most electrocatalysts developed thus far due to poor ORR catalytic activity, whereas the anodic overpotential is usually very small for pure hydrogen. Therefore, the development of cathode catalysts with high ORR activities has been a major issue in fuel cell science and technology. Platinum has been the key catalyst for the ORR, and factors such as alloying with non-precious metals[1–3] and Pt catalyst particle size, contributing to and affecting the ORR activity of Pt, have been investigated extensively. In particular, Yano *et al.* showed that the apparent ORR rate constant and activation energies were independent of particle size in the 1–5 nm range and were identical to those of bulk platinum electrodes.[4] Understanding the ORR mechanism has been a key issue in developing such cathode catalysts with high ORR activities.[5–9] Our recent electrochemical–X-ray photoelectron spectroscopic (EC-XPS) studies have revealed a higher affinity of Pt alloy skin layers compared to pure Pt for oxygen containing adsorbates such as O(ads) and OH(ads) at operating potentials of ORR.[10] This led us (MW, HU) to propose that their increased surface coverage is the origin of the enhanced ORR activities on such alloy catalysts.

The EC-XPS has high sensitivity and specificity in the analysis of the O 1s spectra, with binding energies specific to the various oxygen-containing surface species. On the other hand, being an *ex situ* method, it cannot be combined directly with a simultaneous measurement of ORR activity. *In situ* ATR-FTIR studies[11,12] have been conducted on a Pt film chemically deposited on Si in order to examine the nature of reaction intermediates of ORR in alkaline solution (pH = 11); a band located around 1010 cm^{-1} was observed under oxygen atmosphere and was assigned to the O–O stretch of the superoxide anion, O_2^-, acting as the intermediate of the 4-electron ORR.[12] Baranton *et al.* reported an *in situ* IRAS study utilizing a Nafion® 115 membrane electrolyte (130-μm thickness) to examine the ORR at 0.5 V (RHE) on an iron phthalocyanine (α-FePc) catalyst supported on a carbon substrate.[13] They were able to detect the ν(OH) and δ(HOH) bands of the product water of the ORR around 3450 cm^{-1} and 1620 cm^{-1}, as well as a strong and a weak band at 1050 and 1130 cm^{-1}, respectively. The latter two were assigned to the O–O vibrations of the adsorbed intermediates of the ORR, *i.e.*, O_2H and O_2^-, respectively. Based on the relative band intensities, the step to produce O_2H from O_2^- was ascribed to the rate-determining step (rds) of the ORR on the α-FePc catalyst. That work was the first successful application of IRAS to utilize a Nafion® membrane as the electrolyte; however, the decreased energy throughput of the system, due to the strong infrared absorbance of the thick membrane, was a limitation.

The aim of the present report is first to develop an ATR-FTIR method specifically for use with solid polymer electrolyte membranes that allows us to conduct an *in situ* examination of the catalyst surface under defined electrochemical conditions. Being an ATR method, it is free from the strong infrared absorbance of the membrane electrolyte.

[a] *Fuel Cell Nanomaterials Center, University of Yamanashi, 4 Takeda, Kofu 400-8510, Japan. E-mail: m-watanabe@yamanashi.ac.jp*
[b] *Interdisciplinary Graduate School of Medicine and Engineering, University of Yamanashi, 4 Takeda, Kofu 400-8510, Japan*
[c] *Clean Energy Research Center, University of Yamanashi, 4 Takeda, Kofu 400-8510, Japan*

This is an extension of the *in situ* ATR-FTIR[14–17] and SEIRAS (surface enhanced infrared reflection absorption spectroscopy)[16,18–22] techniques developed for studying electrode surfaces in aqueous electrolytes. Secondly, we intended to apply the new method to the characterization of the interface between a platinum electrode and the Nafion membrane under ORR conditions with potential sweep or steps. We were able to monitor the bands of water, as well as those for an adsorbed reaction intermediate, as a function of potential under ORR conditions.

2. Experimental

We employed an ATR-FT-IR method combined with potential step or cyclic voltammetric (CV) measurements for *in situ* monitoring of the processes associated with ORR on a chemically deposited Pt film (20 × 25 mm) on an Si ATR prism. In order to improve the ionic contact of the Pt film electrode with the Nafion® membrane itself, we cast a 0.1 μm thick Nafion® interlayer by pipetting a measured amount of diluted Nafion® solution (Aldrich) on the Pt film, followed by drying and heat treatment in air at 130 °C for 2 h. The method of chemical deposition of a Pt thin film on the Si ATR prism has been described elsewhere.[19,20] The structure of such a Pt film was examined by SEM and AFM.[20] The film consists of Pt nanoparticles with an average dimension of 100 nm and an estimated thickness of *ca.* 50 nm. It has been known that the electrochemical properties of such a Pt film are very similar to those of ordinary polycrystalline Pt electrodes, as reported for the adsorption/oxidation of CO[14,20,21] and hydrogen.[16,18,19]

We present a schematic view of the cell in Fig. 1, which is based on a carbon separator with an interdigitated-type gas flow field. The counter electrode is a gas-diffusion electrode, which consists of hydrophobic carbon paper with a Pt/C catalyst layer, for which the Pt loading was *ca.* 0.4 mg cm^{-2}. The counter electrode was placed on the flow field with the catalyst layer facing up. A NRE®211 membrane was placed on the same catalyst layer as the electrolyte so that it was sandwiched by the counter and Pt test electrodes. A 20-μm thick gold foil was placed between the Pt electrode and the membrane as a current collector. The reference electrode was a gas diffusion electrode similar to the counter electrode and was fed either with humidified H_2 or O_2. In the former case, it served as a reversible hydrogen electrode (RHE), and some experiments in N_2 and O_2 atmospheres were conducted by use of the RHE. However, most of the measurements under O_2 atmosphere were conducted by use of the reference electrode also under O_2 atmosphere, and the potentials thus measured were converted to the RHE scale by adding the estimated reference potential of 1.1 V *vs.* RHE. Therefore, all potentials are referred to RHE in this report. The O_2 fed to the gas flow field flowed into the counter electrode and then diffused through the NRE®211 membrane to reach the Pt test electrode. In other words, the rate of O_2 supply to the test electrode was defined by that of O_2 diffusion through the membrane. The H_2 and O_2 gases were humidified by a 30-cm-deep bubbler at room temperature which contained either Milli-Q H_2O or D_2O. The O_2 humidified by D_2O was used as an aid to the assignment of the observed spectra, as explained later, as well as for the direct measurement of the H/D isotopic effect on the ORR kinetics. D_2O with 99.8 at.% D content (ACROS ORGANICS)) was used for this experiment. The flow rate of O_2 was set at 20 ml min^{-1}.

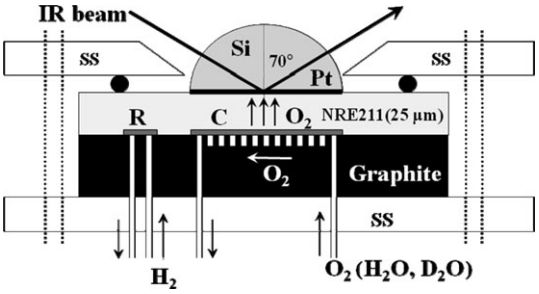

Fig. 1 Experimental set-up to conduct *in situ* ATR-FTIR measurements at the Pt/Nafion interface. The base of the system is a 5 mm thick stainless steel (SS) plate. The thickness of the graphite separator is 20 mm.

The ATR-FTIR measurements were conducted at room temperature by use of a Digilab FTS6000 spectrometer equipped with a broadband MCT detector cooled by liquid nitrogen. The angle of incidence was set at 70°, and the spectral acquisition was conducted by use of unpolarized infrared radiation at 8 cm^{-1} resolution. The interferometer was driven by dry air, which was used for purging the spectrometer as well. The spectral results are displayed in absorbance units, defined as $-\log(I/I_0)$, where I and I_0 represent the spectral intensities in the sample and reference states, respectively. The reference spectrum was collected at 1.1 V (*vs.* RHE) under N_2 or O_2 atmosphere.

We need the information of the vibrational spectra of the membranes for the interpretation of the *in situ* ATR-FTIR spectra at the Pt and electrolyte interfaces as obtained above. Therefore, ATR spectra of Nafion®112 and NRE®211 were measured by use of the same set-up shown in Fig. 1, where the membranes were contacted directly on the surface of the Si ATR prism without a Pt film. For the measurement of the background spectrum, we utilized a reflective aluminium foil in place of the membrane.

2. Results and discussion

2.1 ATR spectra of Nafion® 112 and NRE®211

We present the ATR spectra of the Nafion®112 and NRE®211 membranes in Fig. 2 measured by the setup shown in Fig. 1. There are no significant differences between the spectra for two membranes, which are manufactured by slightly different fabricating procedures, *i.e.*, extrusion and casting methods, respectively. The asymmetric and symmetric CF_2 stretch modes, $\nu_{as}(CF_2)$ and $\nu_s(CF_2)$, at 1213 cm^{-1} and 1153 cm^{-1}, and symmetric SO_3 stretch mode, $\nu_s(SO_3)$, at 1056 cm^{-1} are consistent with those reported for cast Nafion® films and membranes.[23] The water bands around 3460 cm^{-1} and 1600–1700 cm^{-1} are relatively weak as compared to those of CF_2 bands, suggesting that the surface of the membrane sampled by the ATR measurements is rather dry. When measured in the transmission mode, however, the relative intensity of the water bands was significantly enhanced

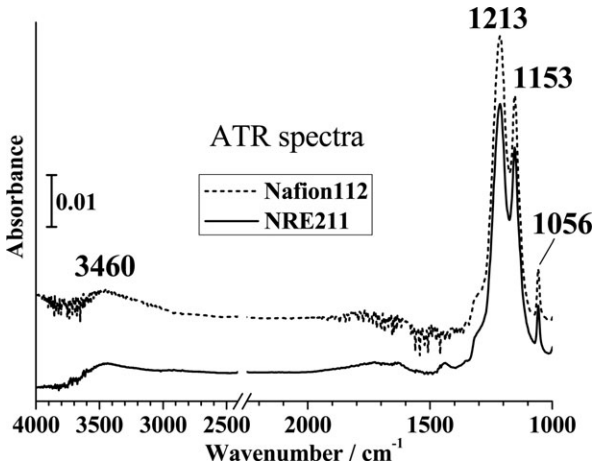

Fig. 2 ATR-FTIR spectra of Nafion 112 and NRE 211 membranes observed in air.

(data not shown). This implies that the water content in the bulk of the membrane is much higher than its surface. This is reasonable as the membranes were placed in the sample compartment of the FTIR purged by dry air.

2.2 CV of the Pt electrode contacted with the cast Nafion® film

Fig. 3 shows a CV observed at the Pt electrode under N_2 atmosphere at 50 mV s^{-1}. The potential sweep was initiated from 0.07 V to avoid an effect of noticeable hydrogen evolution at lower potentials. The resulting hydrogen adsorption and desorption waves were well defined, and the roughness factor, calculated from the hydrogen desorption charge, $_{S}Q_{H}$, and the geometrical area of the Pt film, 5 cm^2, was 5.6. This is slightly smaller than that obtained in electrolyte solutions for a similar Pt film without a Nafion® film, but it is reasonable for the presence of the film to reduce the electrochemically active area by more than 10%.[11]

2.3 ATR-FTIR spectra observed by potential sweep and step methods

Fig. 4 shows ATR-FTIR spectra observed at the Pt electrode contacted with the cast Nafion® film during the CV measurement from 1.175 V (RHE) to 0.175 V in O_2 atmosphere at 1 mV s^{-1}. Spectra were acquired every 50 s, *i.e.*, the potential resolution

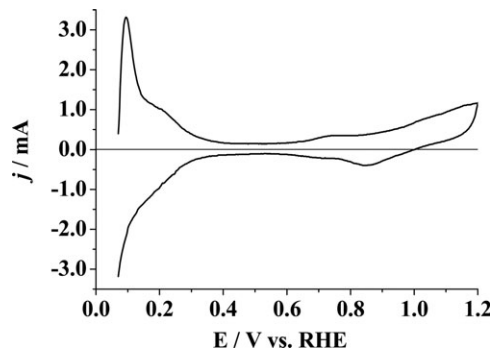

Fig. 3 A CV of the Nafion-coated Pt film electrode on a Si prism observed at 50 mV s^{-1} in N_2 atmosphere humidified by H_2O.

was 50 mV. The CV observed simultaneously is shown in Fig. 5. We can notice the development of the water ν(OH) and δ(HOH) bands around 3500 and 1610 cm^{-1} in (A) and (B), respectively, and of two more bands around 1403 and 1223 cm^{-1} in (B) during the negative-going potential sweep. Of these observed bands, we assign the water bands to the water associated both with the reduction of the Pt surface oxide and that associated with the ORR, based on their development with decreasing electrode potential and increasing ORR current, as shown in Fig. 5. The band around 1223 cm^{-1} can be assigned to the CF_2 stretch modes of the NRE®211 membrane based on its ATR spectra, shown in Fig. 2. The observed development of the CF_2 stretch bands at the lower potentials suggests a change in orientation of Nafion®. This may be associated with incorporation of water produced by the reduction of Pt surface oxides and by the ORR. However, as we have found that the CF_2 stretch modes decrease their intensity upon water incorporation into Nafion®,[24] we assign the change in orientation to an effect of potential. The reason why Nafion® changes its orientation with potential is not clear yet. It may be related to the behavior of the pendant chains containing the SO_3^- group, which is expected to show potential-dependent adsorption/orientation on Pt. Unfortunately, however, the band ascribed to the symmetric SO_3 stretch mode around 1056 cm^{-1} was not clearly detected in Fig. 4. This is the region where the intensity of the incident infrared light is very low due to strong absorption by the massive Si prism window. Therefore, detection of a weak band of the SO_3 stretch mode in this wavenumber region is not expected to be easy. It should be noted here that there is another unassigned band around 1450 cm^{-1} in Fig. 4. We examined the behavior of this band carefully and assigned it to an artifact in the measurement. The band is much less pronounced in Fig. 6, to be shown below, observed by the potential step method, which gave rise to spectra with an improved signal to noise (S/N) ratio and spectral base line compared to Fig. 4, as explained later.

The band around 1403 cm^{-1} develops with decreasing electrode potential and increasing ORR current, but it clearly reaches a maximum, followed by a rapid decrease at lower potentials, as seen in Fig. 4. The band areas, integrated intensities, of the 3500 cm^{-1} for the water band and the 1403 cm^{-1} band were determined and plotted as a function

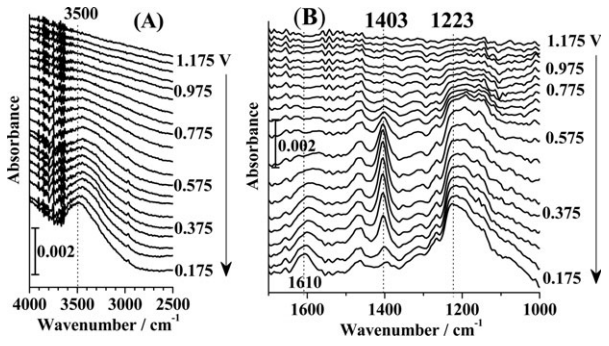

Fig. 4 ATR-FTIR spectra observed during CV measurement at 1 mV s^{-1} on the Nafion-coated Pt in O_2 atmosphere humidified by H_2O. The spectra are referenced to that obtained at 1.2 V.

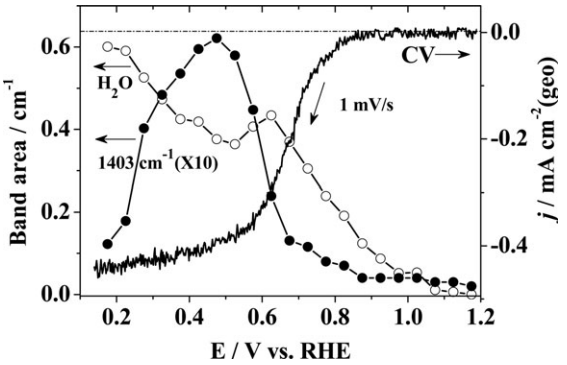

Fig. 5 Potential dependences of the integrated intensity of the 1403 cm^{-1} and 3500 cm^{-1} bands, respectively, and the CV observed at 1 mV s^{-1} simultaneously with ATR-FTIR spectra in O_2 atmosphere humidified by H_2O.

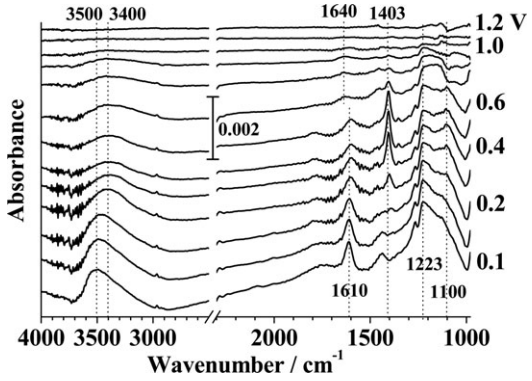

Fig. 6 ATR-FTIR spectra observed at constant potentials on the Nafion®-coated Pt in O_2 atmosphere humidified by H_2O. The spectra are referred to 1.2 V.

of the potential in Fig. 5, in which the observed CV is plotted also as an aid in the interpretation of the intensity data. The intensities of the two bands began to develop from *ca.* 0.9 V at the onset of the ORR. The former band showed a first peak at *ca.* 0.65 V followed by further increase, and finally reached the second peak in the limiting current region of the ORR. It is probable that the increase of adsorbed water can be mainly attributed to the increase in ORR current but a partial contribution of water formed by the reduction of Pt surface oxides in the potential region, *i.e.*, from *ca.* 1.0 to 0.6 V, corresponding to the first peak. The 1403 cm^{-1} band showed a clear maximum around 0.475 V. The potential dependence of the intensity of the 1403 cm^{-1} band will be discussed later.

We conducted further measurements by a potential step method to confirm the results observed by the potential sweep method described above. After acquiring a background spectrum at 1.2 V, the potential was stepped to lower potentials, at which sample spectra were observed. For these potential step measurements, 500 interferometer scans were conducted at each potential E and were averaged to improve the S/N ratio. Fig. 6 shows a series of spectra observed at various potentials. The change of the spectra with potential was very similar to that observed by the potential sweep method shown in Fig. 4. Owing to the improved quality of the baseline, however, we can notice a shift of the water band, ν(OH), from

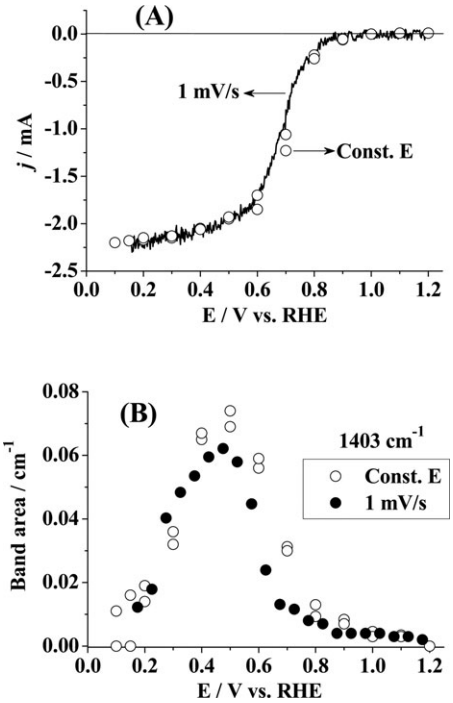

Fig. 7 Comparison of the data observed by a potential sweep at 1 mV s^{-1} and at steady-state (constant potential) in O_2 atmosphere humidified by H_2O. (A) Current *vs.* potential and (B) 1400 cm^{-1} band area *vs.* potential.

ca. 3400 to 3500 cm^{-1} below 0.4 V. We have conducted comparisons of the current–potential (I–E) curves and the band intensity data, obtained by the potential sweep and potential step methods. Fig. 7 presents results of the comparison of the I–E data in (A) and the intensities of the 1403 cm^{-1} band in (B). We can conclude a close agreement between the data obtained by the two methods.

2.4 ATR-FTIR spectra observed with a D_2O bubbler

The assignment of the 1403 cm^{-1} band described above is still uncertain. The good correspondence between its band intensity and the ORR current depicted in Fig. 5 and also Fig. 7 suggests that the species giving rise to the band is closely associated with the ORR, *i.e.*, either a reactant species or an intermediate. We will discuss this issue in what follows. Historically, several intermediate species of the ORR have been proposed in association with the associative and dissociative mechanisms of ORR,[25] *i.e.*, adsorbed O_2,[25] O_2^-,[12,13] O_2H,[13,26] OH and O.[10] Of these intermediates, adsorbed OH and O can be excluded, as the frequency, 1403 cm^{-1}, is too high for vibrations associated with these species (discussed later). The other three species, O_2, O_2^-, and O_2H have O–O vibrations ranging from 1555 cm^{-1} (Raman, O_2) to 1097 cm^{-1} (O_2^-) and 1389, 1101 cm^{-1} (ν_2 and ν_3, O_2H).[27] The frequencies for O_2^- and O_2H were determined by the matrix isolation method utilizing an inert gas matrix, whereas the Raman active O–O frequency of O_2 was determined in the gas phase.

Because it is difficult to predict the shifts of these frequencies for species adsorbed on electrodes, we thought that it would be

useful to know if the species associated with the 1403 cm^{-1} vibration includes a hydrogen atom. This question can be answered by examining the frequency shift upon changing from H_2O to D_2O humidification. There would be no shift for such species as adsorbed O_2 and O_2^-, but we would expect a red shift of *ca.* 16 cm^{-1} for the O_2D species due to its increased reduced mass compared to O_2H.

In Fig. 8, we compare the spectra observed at 0.4 V with a H_2O and D_2O bubbler. The spectrum for D_2O was referred to the background spectrum acquired at 1.2 V after the replacement from H_2O to D_2O had been completed. The replacement took place in the electrolyte and the electrolyte/Pt interface by counter-diffusion of H_2O and D_2O and by exchanging H^+ with D^+ formed by the electrochemical reactions given below for *ca.* 1 h, as shown later.

$$D_2O \rightarrow 2D^+ + 2e + 1/2O_2 \text{ at the counter electrode}$$

$$-SO_3H + D^+ \rightarrow -SO_3D + H^+ \text{ in the electrolyte}$$

$$2H^+ + 2e + 1/2O_2 \rightarrow H_2O \text{ at the working electrode}$$

$$2D^+ + 2e + 1/2O_2 \rightarrow D_2O \text{ at the working electrode}$$

We notice that the ν(OH) and δ(HOH) bands at 3380 and 1600 cm^{-1}, respectively, observed with a H_2O bubbler are absent, and there is a new ν(OD) band at 2642 cm^{-1}, whereas the 1403 cm^{-1} band has not shifted at all. These results clearly indicate, firstly, that the water associated with the ORR was produced from O_2 and D^+ ions in equilibrium with D_2O vapor supplied through the bubbler, and secondly, that the species responsible for the 1403 cm^{-1} band includes no hydrogen atom.

In Fig. 9, we show the potential dependence of the integrated intensities of the 1403 cm^{-1} band and product D_2O, and the CV observed under D_2O humidification. The result is very similar to that presented in Fig. 5 under H_2O humidification. However, the potential of the peak intensity of the 1403 cm^{-1} band and the CV are shifted to lower potentials than those observed for H_2O humidification. This is due to the slower kinetics of ORR on Pt in D_2O and is a direct evidence of the involvement of a proton in the rds, *i.e.*, a proton-coupled electron transfer process (PCET).[28] This type of

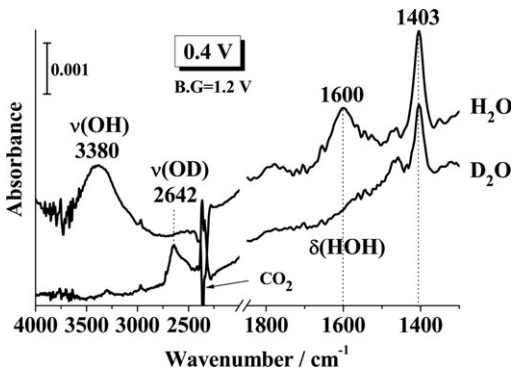

Fig. 8 Change of the spectra from H_2O to D_2O humidification at 0.4 V in O_2 atmosphere. The spectra are referenced to those obtained at 1.2 V under H_2O and D_2O humidification, respectively.

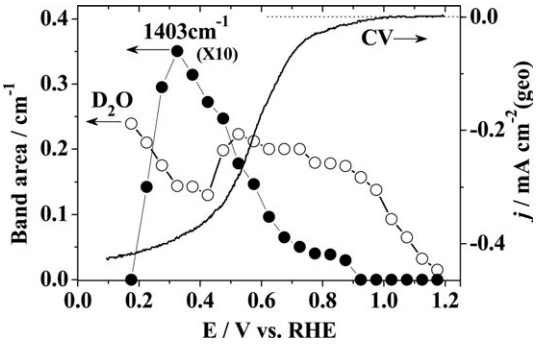

Fig. 9 Potential dependence of the intensities of the 1400 cm^{-1} and D_2O bands and the CV at 1 mV s^{-1} observed under D_2O humidification in O_2 atmosphere.

process is consistent with the ORR mechanistic pathway for Pt in acid proposed by Wang *et al.*[29] It is in contrast to results for the ORR on Hg, in which the initial electron transfer step exhibits no H/D effect.[30] We should also mention that a recent paper reported an H/D separation factor for the ORR in a PEFC as a practical means of isotope separation.[31]

We also should report that we have found another type of water band during the H_2O/D_2O replacement experiment. We followed the replacement process at 0.5 V for 1 h after acquiring a background spectrum at 1.2 V. The time resolution of the measurement was set at 2 min, during which 1080 interferograms were collected and averaged. Fig. 10 shows the evolution of the spectra during this time. The initial spectrum acquired at $t = 0$ in $O_2(H_2O)$ has bands at 3440 and 1600 cm^{-1} assigned to ν(OH) and δ(HOH) vibrations, respectively, of the water associated with the ORR. After switching to a D_2O bubbler, these initial water bands are absent by *ca.* 4 min, and we start seeing the development of a new positive-going band at 2494 cm^{-1} and negative-going ones around 3230–3373 and 1630 cm^{-1}. The 2494 cm^{-1} band is assigned to the ν(OD) vibration of D_2O in the deuterated Nafion® film,[23] but it should be noted that its intensity is much higher than that of the initial ν(OH) band replaced. This implies that the band contains a contribution of the D_2O gain in the Nafion® layer on Pt, in addition to the product D_2O of the ORR. Note that its peak frequency, 2494 cm^{-1} is 148 cm^{-1} lower, and the final intensity several times higher, respectively, than those of the product D_2O, as seen in Fig. 8. The negative-going water bands around 3230–3373 cm^{-1} and 1630 cm^{-1} can then be ascribed to the ν(OH) and δ(HOH) vibrations of H_2O, originally present in the Nafion® layer, that are replaced by those associated with D_2O. The δ(HOH) frequency, 1630 cm^{-1}, is in agreement with that reported by Korzeniewski *et al.* for a relatively dry condition, with an H_2O/SO_3^- ratio of *ca.* 3.[32] Therefore, we can conclude that the procedure to change from H_2O to D_2O humidification presents a new unique method to observe the absolute spectra of the water *in situ* at the Pt/Nafion interface without referring to any background states.

The lower ν(OH) and ν(OD) and higher δ(HOH) frequencies of H_2O and D_2O in the Nafion layer compared with those of the water associated with ORR can probably be ascribed to the different locations of the water. Naturally, the H_2O or D_2O

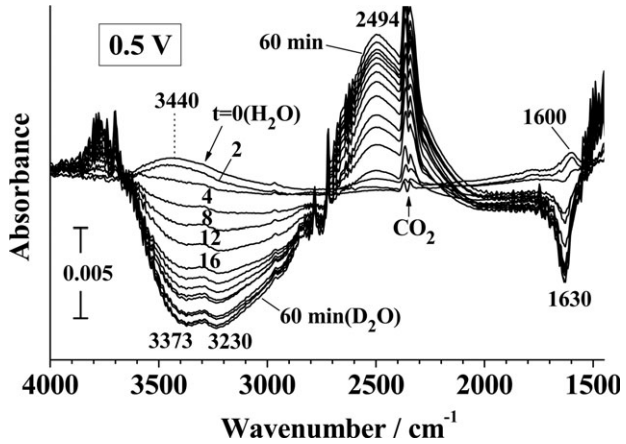

Fig. 10 Change of the ATR-FTIR spectra during the H_2O-to-D_2O humidification change at 0.5 V. The spectra were acquired every 2 min and referenced to that obtained at 1.2 V under H_2O humidification.

produced by ORR is located closer to the Pt surface than the water present in the Nafion layer. This interpretation is supported by the potential dependent ν(OH) and δ(HOH) frequencies of the product water, as depicted in Fig. 6.

We further examined the contribution of ORR current to the rate of the H_2O/D_2O replacement. For this, the replacement was monitored at 1.2 V, *i.e.*, in the absence of ORR current, when the bubbler was switched from D_2O to H_2O. Fig. 11 shows the development of positive-going ν(OH) and δ(HOH) bands at 3230–3368 cm^{-1} and 1630 cm^{-1}, respectively, accompanied by the negative-going ν(OD) band at 2493 cm^{-1} during the replacement of D_2O by H_2O in the Nafion layer on Pt. The H_2O/D_2O replacement in the presence and absence of ORR current can be compared in a quantitative way by monitoring the change of the 1630 cm^{-1} band intensity with time. The ν(OH) and ν(OD) bands are overlapped in opposite directions, making it difficult to determine their individual band intensities, whereas the δ(HOH) band at 1630 cm^{-1} is not overlapped with the δ(DOD) band to be located around 1200 cm^{-1}. The latter band is not seen clearly, due to the overlapping $\nu(CF_2)$ band of the Nafion® backbone in this region.

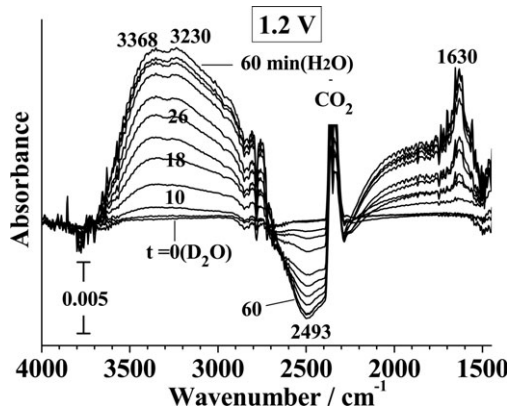

Fig. 11 Change of the ATR-FTIR spectra during D_2O-to-H_2O humidification change at 1.2 V in O_2 atmosphere. The spectra were acquired every 2 min and referenced to that obtained at 1.2 V under D_2O humidification.

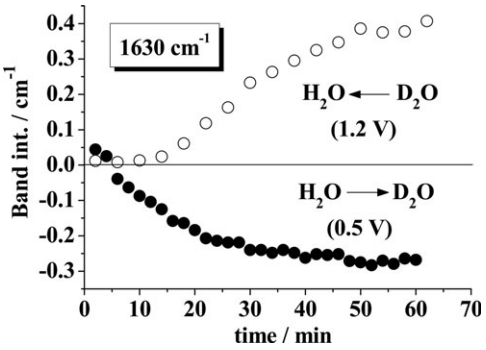

Fig. 12 Change of the band intensity of the water bending mode (1630 cm^{-1}) band after switching the humidification from D_2O to H_2O at 1.2 V and from H_2O to D_2O at 0.5 V in O_2 atmosphere.

Fig. 12 compares the intensities of the 1630 cm^{-1} band at 1.2 V and 0.5 V, *i.e.*, in the absence and presence of an ORR current of −2 mA, during the H_2O/D_2O replacement experiments. At 0.5 V, the band intensity reaches a steady value within *ca.* 30 min, whereas the rate of the band intensity increase is significantly lower at 1.2 V. The contribution of the ORR current is clearly seen in the enhanced rate of H_2O/D_2O replacement observed at 0.5 V. We estimated the time required to replace all protons and H_2O molecules in the NRE® 211 membrane (20 × 25 mm × 25 μm) + cast Nafion® film (20 × 25 mm × 0.1 μm) by the −2 mA ORR current. The equivalent ion exchange capacity (0.89 meq/g) and density (2 g cm^{-3}) of the Nafion were employed, resulting in *ca.* 18 min to replace all protons by D^+. In addition to the protons, we have to replace the water molecules in the membrane, the latter being expected to vary with relative humidity. The bubbler was operated at room temperature in the present study, and accordingly, the humidity was low. Therefore, the period of *ca.* 0.5 h required to replace H_2O by D_2O at 0.5 V is in reasonable agreement with that estimated above.

Finally, we noticed that the spectra of the new water bands observed at 0.5 and 1.2 V as a result of H_2O/D_2O replacement were nearly identical to those shown in Fig. 10 and 11. The bands appeared in opposite directions, due to the different replacement procedures, but exhibited comparable band intensities and nearly identical ν(OH), ν(OD) and δ(HOH), δ(DOD) frequencies. The absence of potential dependence suggests that most of the H_2O and D_2O contributing to the spectra were not adsorbed at the Pt/Nafion interface but were located in the bulk of the cast Nafion® film.

2.5 Comparison between N_2 and O_2 atmospheres

We then sought to establish whether or not the 1403 cm^{-1} band is specific to the ORR by conducting the ATR-FTIR measurement under an N_2 atmosphere. For this experiment, we employed an RHE by supplying humidified H_2 gas to the reference electrode. In Fig. 13, we show the spectra observed at 0.675 V (RHE) under O_2 and N_2 atmospheres. For O_2, we see a clear band at 1400 cm^{-1}, whereas such a band is absent for N_2. The peak wavenumber, 1400 cm^{-1}, was lower than the 1403 cm^{-1} observed in Fig. 4, but these values coincide within the spectral resolution of 8 cm^{-1}. We can conclude, therefore,

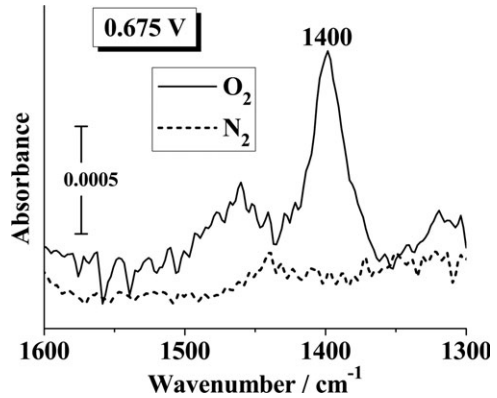

Fig. 13 Comparison of the ATR-FTIR spectra observed at 0.675 V under O_2 and N_2 atmospheres. The spectra are referenced to that obtained at 1.1 V.

that the 1400–1403 cm^{-1} band observed under O_2 atmosphere is associated with the ORR.

3. Discussion

3.1 Assignment of the 1403 cm^{-1} band and mechanism of the ORR

The 1403 cm^{-1} band exhibited no detectable frequency shift upon changing from H_2O to D_2O humidification, as shown in Fig. 8. This implies that the species responsible for the band contained no hydrogen. Thus, as the main possible candidates, we have either O_2(ads) or O_2^- (ads) to be assigned to this band. Yeager *et al.* proposed an ORR mechanism involving a rate-determining one-electron reduction of O_2 to O_2^- (ads) for cases in which the Tafel slope is *ca.* 120 mV/decade at 25 °C. [33,34] However, the observed frequency, 1403 cm^{-1}, is significantly higher than either the 1130 cm^{-1} or 1005–1016 cm^{-1} values reported by Baranton *et al.*[13] and Shao *et al.*,[12] respectively, for the O_2^- species as a major intermediate of ORR on an iron phthalocyanine (α-FePc) catalyst and on Pt in alkaline solution (pH = 11). It is known that dioxygen in oxyhemoglobin and oxymyoglobin bonds to Fe(II) to form a bent Fe–O–O adduct and exhibits a ν(O–O) frequency close to 1100 cm^{-1}.[35] The frequency is close to that typical for superoxide, which has been taken as an evidence of a substantial transfer of electron density from the iron to the coordinated O_2, giving rise to an Fe(II)–O_2^- configuration. The ν(O–O) frequency for O_2 on α-FePc[13] is consistent with those for dioxygen in oxyhemoglobin and oxymyoglobin, as mentioned above. This frequency, 1130 cm^{-1}, is also very close to that of superoxide ions produced by controlled potential electrolysis in aprotic media, 1140 cm^{-1}.[36] Shao *et al.*[12] supported their result by detecting a similar band around 1010–1018 cm^{-1} on Pt in O_2-saturated acetonitrile, in which the O_2^- species is known to be stable. Their assignment of the band to a bridge-bonded O_2^-, with two bonds to two Pt sites[37,38] is somewhat puzzling, since this orientation should be infrared-inactive, according to the surface selection rule in IRAS[39] as well as ATR-SEIRAS.[40] However, Gland *et al.* noted this difficulty also for electron energy loss spectroscopy (EELS), arguing that the Pt–O stretch (as part of the Pt–O_2 system) mixes considerably with the O–O stretch, making the latter observable.[41]

Now, we will discuss the assignment of the 1403 cm^{-1} band based on data obtained during the reverse scan, as well as mechanistic considerations of the ORR. We have found that the potential dependence of the 1403 cm^{-1} band intensity is a key for its assignment. First, we analyzed the spectra observed during the reverse scan for the experiment under O_2 atmosphere with the use of the RHE. In Fig. 14, we present the CV, (A), and potential dependence of the intensity of the 1400 cm^{-1} band, (B), observed during the forward (negative-going) and reverse scans, denoted as NGS and RS, at 1 mV s^{-1} between 1.1 V and 0.1 V under O_2 atmosphere. The CV and the band intensities both exhibited hysteresis during the scans to maintain higher ORR current and band intensity during the reverse scan above *ca.* 0.75 V. The hysteresis in the CV is probably due to the irreversibility of reduction/formation of Pt surface oxides in NGS/RS, respectively, although it is not severe in the present work, since the scan rate of 1 mV s^{-1} is extremely slow compared to that in most published works. On the other hand, the higher intensity of the 1400 cm^{-1} band above 0.75 V during the RS suggests that the adsorbed species responsible for the band is stable up to 1.1 V at the sweep rate of 1 mV s^{-1}. For O_2^-(ads), this potential would presumably be too positive, and it would be expected to quickly oxidize on Pt or to react with protons in the cast Nafion® film, which serves as a strong acid. In fact, O_2^-(ads) would not be expected to be stable under any conditions examined in the present work. The reversible potential for the O_2/O_2^- redox couple in aqueous solution has a value of *ca.* −0.284 V *vs.* SHE;[33] adsorption could well modify this value somewhat, but we regard it

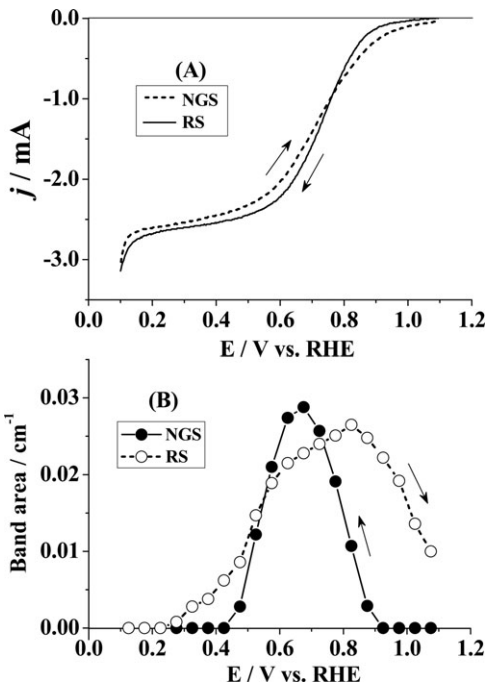

Fig. 14 (A) CV observed at 1 mV s^{-1} during negative-going and reverse scans, denoted as NGS and RS, between 1.1 and 0.1 V under O_2 atmosphere. (B) Potential dependence of the intensity of the 1400 cm^{-1} band observed simultaneously with the CVs in (A).

unlikely that even the adsorbed state would be observable at such high potentials.

To conclude the assignment of the 1400 cm^{-1} band, we assign it to the O–O stretch of the O_2(ads) based on (a) its potential dependence and (b) its much higher frequency than that known for superoxide. According to the surface selection rule,[39,40] the O–O vibration should have a component of the dipole moment change perpendicular to the Pt surface. On this basis, we propose the end-on, somewhat tilted orientation of the adsorbed O_2 molecule on Pt, which was originally proposed by Pauling[42,43] for the iron–oxygen bond in oxyhemoglobin. The observed red shift of the O–O stretching frequency by 155 cm^{-1} from that of O_2 in gas phase, 1555 cm^{-1},[27] is interpreted in terms of a partial charge transfer between adsorbed O_2 and Pt of a value less than unity. The balance between electron donation from the O_2 3σ orbital to an empty Pt $5d_{z^2}$ orbital and back-donation from Pt $5d_{xy}$ or $5d_{yz}$ orbitals to an antibonding π^* orbital of O_2 would lead to weakening the O–O bond and thus lowering of its vibrational frequency.

A Pauling-type adsorbed O_2 molecule, with a partial charge of approximately -0.5, appears to be the simplest explanation for the present experimental results. However, we are puzzled by the fact that this vibrational frequency (*ca.* 1400 cm^{-1}) has not been observed for the simple case of molecular O_2 adsorption on well-defined platinum surfaces in any of the surface science literature of which we are aware, including EELS[41,44] and IRAS[45] studies of O_2 adsorption on Pt(111) in ultrahigh vacuum. In those studies at relatively low temperature (<100 K), the O_2 molecule has been proposed to be adsorbed in two principal configurations, a superoxo-like, bridging species with the O–O axis parallel to the Pt surface, with the O–O stretching frequency lowered considerably (850–873 cm^{-1}) from that for the neutral state (1555 cm^{-1}), corresponding to a charge of -1 and an O–O bond order of 1.5, and a peroxo-like, lying down but slightly tilted species, with an O–O stretching frequency in the 680–703 cm^{-1} range, a bond order of 1.0 and a charge of -2. Adsorbed oxygen atoms have been found to exhibit a Pt–O stretching peak at *ca.* 490 cm^{-1}.[41,44] However, we note that Steininger *et al.* reported an EELS peak at 1400 cm^{-1} for a case in which there was a high coverage of adsorbed molecular oxygen that was partially converted to atomic oxygen.[44] We intend to follow up this lead in subsequent work, recognizing that the simultaneous presence of adsorbed atomic oxygen can significantly affect the bonding of molecular oxygen to the platinum surface.

Thus far, no theoretical study of which we are aware has described any species that could lead to the observance of an infrared peak at 1400 cm^{-1}. One recent study, however, predicts much smaller charge transfer to the superoxo and peroxo forms of adsorbed O_2 molecule, as little as 0.08 *e*, compared to that previously thought, but still with typical O–O stretching modes, *i.e.*, 913 and 826 cm^{-1}, respectively, for the gas–solid interface.[46] Another recent study[47] has modeled the adsorption of O_2 on Pt(111) in the presence of water molecules and an applied potential, which could be expected to modify the adsorption mode, but found a bridging superoxo-like species to be the most stable, with an O–O stretching mode at 832 cm^{-1}, similar to that found experimentally for UHV.

Based on the assignment given above, we interpret the potential dependence of the 1400 cm^{-1} band during the negative going scan as follows. The Pt surface is partially covered by O(ads) and OH(ads)[10] at the starting potential, 1.1 V, at which O_2 adsorption is limited. As the potential is lowered, however, O(ads) and OH(ads) are electrochemically reduced, decreasing their coverages, enhancing O_2 adsorption and leading to an increase of O_2(ads) coverage. The ORR is promoted by the increase of O_2(ads), which dissociates to O(ads), the latter being the intermediate we have proposed for the rds of ORR, *i.e.*, O(ads) + H^+ + e^- → OH(ads).[10]

Thus, the band intensity change can be explained by taking into account the two different types of O(ads) on Pt, each with its own potential dependence, *i.e.*, one produced by Pt surface oxidation above *ca.* 0.7 V and the other by adsorption/dissociation of O_2, which is enhanced as the surface oxides are reduced below *ca.* 1.0 V. The O(ads) produced by O_2 adsorption/dissociation is the rate limiting reactant of the rds, O(ads) + H^+ + e^- = OH(ads), preceded by the O_2 adsorption/dissociation steps, which are in pre-equilibrium. In the limiting current region, the rds is shifted to the step of O_2 diffusion, resulting in the lowered O_2 (ads) concentration, due to the insufficient diffusion rate. Therefore, the proposed coverage of O_2(ads), and the intensity of the 1400 cm^{-1} band, should exhibit a peak at a potential before the limiting diffusion current region. In fact, this is depicted clearly in Fig. 5 and 14.

4. Conclusion

An infrared band was observed at 1400–1403 cm^{-1} under humidified oxygen atmosphere in close association with ORR current at the Pt/Nafion interface. Its absence in N_2 atmosphere and insensitivity to the change from H_2O to D_2O humidification suggests an assignment of the band to the O–O vibration of O_2(ads). This is the simplest model that could fit the present experimental observations. In subsequent work, we are examining in more detail the interactions between adsorbed molecular oxygen and other adsorbed species such as O(ads) and OH(ads).

The intensity of the band exhibits a peak with increasing ORR current but decreases sharply in the limiting diffusion current region. Such a potential dependence is well explained by an ORR mechanism in which the step to produce O_2(ads) is in equilibrium, *i.e.*, O_2(surface)⇌O_2(ads); the coverage of the latter increases as the surface oxygen species, O(ads) and OH(ads), originally present at 1.1 V are electrochemically reduced at the lower potentials. The band intensity reaches zero when the surface concentration of O_2 becomes negligible under the diffusion-limited conditions.

Acknowledgements

The authors gratefully acknowledge support of this work through the Research on Nanotechnology for High Performance Fuel Cells (HiPer-FC) project of the New Energy and Industrial Development Organization of Japan (NEDO).

References

1 H. Yano, M. Kataoka, H. Yamashita, H. Uchida and M. Watanabe, *Langmuir*, 2007, **23**, 6438–6445.
2 H. Yano, J. M. Song, H. Uchida and M. Watanabe, *J. Phys. Chem. C*, 2008, **112**, 8372–8380.
3 J. Greeley and J. K. Norskov, *J. Phys. Chem. C*, 2009, **113**, 4932–4939.
4 H. Yano, J. Inukai, H. Uchida, M. Watanabe, P. K. Babu, T. Kobayashi, J. H. Chung, E. Oldfield and A. Wieckowski, *Phys. Chem. Chem. Phys.*, 2006, **8**, 4932–4939.
5 T. Toda, H. Igarashi and M. Watanabe, *J. Electrochem. Soc.*, 1998, **145**, 4185–4188.
6 T. Toda, H. Igarashi and M. Watanabe, *J. Electroanal. Chem.*, 1999, **460**, 258–262.
7 T. Toda, H. Igarashi, H. Uchida and M. Watanabe, *J. Electrochem. Soc.*, 1999, **146**, 3750–3756.
8 L.-J. Wan, T. Moriyama, M. Ito, H. Uchida and M. Watanabe, *Chem. Commun.*, 2002, 58–59.
9 H. Uchida, H. Ozuka and M. Watanabe, *Electrochim. Acta*, 2002, **47**, 3629–3636.
10 M. Wakisaka, H. Suzuki, S. Mitsui, H. Uchida and M. Watanabe, *J. Phys. Chem. C*, 2008, **112**, 2750–2755.
11 Y. Ayato, K. Kunimatsu, M. Osawa and T. Okada, *J. Electrochem. Soc.*, 2006, **153**, A203–A209.
12 M.-h. Shao, P. Liu and R. R. Adzic, *J. Am. Chem. Soc.*, 2006, **128**, 7408–7409.
13 S. Baranton, C. Coutanceau, E. Garnier and J.-M. Léger, *J. Electroanal. Chem.*, 2006, **590**, 100–110.
14 K. Kunimatsu, T. Sato, H. Uchida and M. Watanabe, *Electrochim. Acta*, 2008, **53**, 6104–6110.
15 M. Watanabe, T. Sato, K. Kunimatsu and H. Uchida, *Electrochim. Acta*, 2008, **53**, 6928–6937.
16 K. Kunimatsu, T. Senzaki, G. Samjeske, M. Tsushima and M. Osawa, *Electrochim. Acta*, 2007, **52**, 5715–5724.
17 T. Yajima, H. Uchida and M. Watanabe, *J. Phys. Chem. B*, 2004, **108**, 2654–2659.
18 K. Kunimatsu, T. Senzaki, M. Tsushima and M. Osawa, *Chem. Phys. Lett.*, 2005, **401**, 451–454.
19 K. Kunimatsu, H. Uchida, M. Osawa and M. Watanabe, *J. Electroanal. Chem.*, 2006, **587**, 299–307.
20 A. Miki, S. Ye and M. Osawa, *Chem. Commun.*, 2002, 1500–1501.
21 Y. X. Chen, A. Miki, S. Ye, H. Sakai and M. Osawa, *J. Am. Chem. Soc.*, 2003, **125**, 3680–3681.
22 S. Pronkin and T. Wandlowski, *Surf. Sci.*, 2004, **573**, 109–127.
23 A. Gruger, A. Régis, T. Schmatko and P. Colomban, *Vib. Spectrosc.*, 2001, **26**, 215–225.
24 K. Kunimatsu, H. Uchida and M. Watanabe, to be submitted.
25 J. K. Norskov, J. Rossmeisl, A. Logadottir, L. Lindqvist, J. R. Kitchin, T. Bligaard and H. Jónsson, *J. Phys. Chem. B*, 2004, **108**, 17886–17892.
26 N. Wakabayashi, M. Takeichi, H. Uchida and M. Watanabe, *J. Phys. Chem. B*, 2005, **109**, 5836–5841.
27 K. Nakamoto, *Infrared and Raman Spectra of Inorganic and Coordination Compounds, Part A*, Wiley-Interscience, New York, 1997.
28 R. I. Cukier and D. G. Nocera, *Annu. Rev. Phys. Chem.*, 1998, **49**, 337.
29 J. X. Wang, J. Zhang and R. R. Adzic, *J. Phys. Chem. A*, 2007, **111**, 12702–12710.
30 C. J. Van Velzen, J. M. Oostveen, M. Sluyters-Rehbach and J. H. Sluyters, *J. Electroanal. Chem.*, 1985, **191**, 175–183.
31 M. P. M. Kaninski, V. M. Nikolic, A. D. Maksic, G. S. Tasic and S. S. Miljanic, *Electrochem. Commun.*, 2008, **10**, 1463–1466.
32 C. Korzeniewski, D. E. Snow and R. Basnayake, *Appl. Spectrosc.*, 2006, **60**, 599–604.
33 M. R. Tarasevich, A. Sadkowski and E. Yeager, in *Kinetics and Mechanisms of Electrode Processes*, ed. B. E. Conway, J. O. M. Bockris, E. Yeager, S. U. M. Khan and R. E. White, Plenum Press, New York, 1983, vol. 7, pp. 301–398.
34 E. R. Yeager, M. Gervasio, D. Razaq, A. Tryk and D., in *Structural Effects in Electrocatalysis and Oxygen Electrochemistry*, ed. D. Scherson, D. Tryk, M. Daroux and X. Xing, The Electrochemical Society Inc., Pennington, NJ, 1992, vol. PV 92-11, p. 440.
35 M. Tsubaki and N. T. Yu, *Proc. Natl. Acad. Sci. U. S. A.*, 1981, **78**, 3581–3585.
36 D. Vasudevan and H. Wendt, *J. Electroanal. Chem.*, 1995, **392**, 69–74.
37 E. Yeager, *J. Electrochem. Soc.*, 1981, **128**, 160C–171C.
38 R. R. Adzic and J. X. Wang, *J. Phys. Chem. B*, 1998, **102**, 8988–8993.
39 F. M. Hoffmann, *Surf. Sci. Rep.*, 1983, **3**, 107.
40 M. Osawa, K.-I. Ataka, K. Yoshii and Y. Nishikawa, *Appl. Spectrosc.*, 1993, **47**, 1497–1502.
41 J. L. Gland, B. A. Sexton and G. B. Fisher, *Surf. Sci.*, 1980, **95**, 587–602.
42 L. Pauling and C. D. Coryell, *Proc. Natl. Acad. Sci. U. S. A.*, 1936, **22**, 210–216.
43 L. Pauling, *Nature*, 1964, **203**, 182–183.
44 H. Steininger, S. Lehwald and H. Ibach, *Surf. Sci.*, 1982, **123**, 1–17.
45 K. Gustafsson and S. Andersson, *J. Chem. Phys.*, 2004, **120**, 7750–7754.
46 L. Qi, X. Qian and J. Li, *Phys. Rev. Lett.*, 2008, **101**, 146101–146104.
47 M. J. Janik, C. D. Taylor and M. Neurock, *J. Electrochem. Soc.*, 2009, **156**, B126–B135.